Journal of Biomedical Optics

BiomedicalOptics.SPIEDigitalLibrary.org

In vivo evaluation of battery-operated light-emitting diode-based photodynamic therapy efficacy using tumor volume and biomarker expression as endpoints

Srivalleesha Mallidi
Zhiming Mai
Imran Rizvi
Joshua Hempstead
Stephen Arnason
Jonathan Celli
Tayyaba Hasan

SPIE.

In vivo evaluation of battery-operated light-emitting diode-based photodynamic therapy efficacy using tumor volume and biomarker expression as endpoints

Srivalleesha Mallidi,[a] Zhiming Mai,[a] Imran Rizvi,[a,b] Joshua Hempstead,[c] Stephen Arnason,[c] Jonathan Celli,[c] and Tayyaba Hasan[a,*]
[a]Massachusetts General Hospital, Wellman Center for Photomedicine, 40 Blossom Street, Boston, Massachusetts 02114, United States
[b]Brigham and Women's Hospital, Department of Medicine, Boston, Massachusetts, United States
[c]University of Massachusetts, Department of Physics, 100 Morrissey Boulevard, Boston, Massachusetts 02125, United States

Abstract. In view of the increase in cancer-related mortality rates in low- to middle-income countries (LMIC), there is an urgent need to develop economical therapies that can be utilized at minimal infrastructure institutions. Photodynamic therapy (PDT), a photochemistry-based treatment modality, offers such a possibility provided that low-cost light sources and photosensitizers are available. In this proof-of-principle study, we focus on adapting the PDT light source to a low-resource setting and compare an inexpensive, portable, battery-powered light-emitting diode (LED) light source with a standard, high-cost laser source. The comparison studies were performed *in vivo* in a xenograft murine model of human squamous cell carcinoma subjected to 5-aminolevulinic acid-induced protoporphyrin IX PDT. We observed virtually identical control of the tumor burden by both the LED source and the standard laser source. Further insights into the biological response were evaluated by biomarker analysis of necrosis, microvessel density, and hypoxia [carbonic anhydrase IX (CAIX) expression] among groups of control, LED-PDT, and laser-PDT treated mice. There is no significant difference in the percent necrotic volume and CAIX expression in tumors that were treated with the two different light sources. These encouraging preliminary results merit further investigations in orthotopic animal models of cancers prevalent in LMICs. [DOI: 10.1117/1.JBO.20.4.048003]

Keywords: photodynamic therapy; δ-aminolevulinic acid; protoporphyrin IX; global health; light emitting diode; necrosis; microvessel density; carbonic anhydrase IX.

Paper 140415RR received Jun. 29, 2014; accepted for publication Mar. 30, 2015; published online Apr. 24, 2015.

1 Introduction

In low- to middle-income countries (LMICs), the rates of cancer occurrence and cancer-related mortality are increasing at paces that will exceed such rates in more developed countries.[1] In a study of cancer-specific patterns and trends, Bray et al. predict an increase in cancer incidence from the 12.7 million new cases in 2008 to 22.2 million cases by 2030, and with the rapid socioeconomic transition of LMICs toward westernization, countries might see a reduction in infection-related cancers but an increase in reproductive, dietary, or hormonal related cancers.[2] With the rise of cancer occurrence and cancer-related mortality, the GLOBOCAN initiative and several recent articles indicate the need for closing the disproportional gap between cancer incidence and mortality rates in developed countries and LMICs.[3–5] Several countries have already taken the initiative to bridge this gap, and a Global Task Force has been created to increase the accessibility of cancer in LMICs.[3] To solve this particular global cancer challenge, it is critical to develop cancer diagnostic and therapeutic techniques that are inexpensive and can be used in low-resource settings.

Surgery, radiation, and chemotherapy are the mainstays of cancer management, yet they require major medical infrastructure and are costly for both the patient and the society. Therefore, there is a need for an alternative approach to these high-cost procedures. Photodynamic therapy (PDT) is one such option and has shown promise in treating several types of cancers that are prevalent in LMICs, such as oral, bladder, glioma, pancreatic, and esophageal cancers. PDT is a photochemistry-based modality that imparts light-mediated cytotoxicity to target tissues via excitation of a photosensitizer with light of a specific wavelength.[6–8] The technique is clinically approved for the treatment of a number of carcinomas, and the mechanisms of action have been well studied.[6,9]

The two major components that need to be available for the successful implementation of PDT in LMICs are affordable photosensitizers and light sources. The prodrug δ-aminolevulinic acid (ALA), which preferentially converts to the photosensitizer protoporphyrin IX (PpIX) in tumors, can be stored at room temperature without specialty storage equipment. ALA can be easily administered to patients topically, as a cream, or orally, through ingestion in beverages, without sophisticated medical setups or highly trained healthcare professionals. Moreover, ALA is readily available in LMICs such as India (DUSA Pharmaceuticals, Inc., a subsidiary of Sun Pharmaceutical Industries Ltd., an India-based conglomerate). The second major component of PDT is the light source required to initiate photodynamic action.[10] Often, light sources are expensive, bulky, and immobile. Moreover, current PDT light sources (e.g., lasers) typically require electricity for

*Address all correspondence to: Tayyaba Hasan, E-mail: thasan@mgh.harvard.edu

continuous operation, a feature not available in developing countries due to frequent electrical power failure. In recent years, there have been several attempts to replace lasers with light-emitting diode (LED)-based light sources to reduce cost and increase flexibility of use in sites outside major hospitals.[11] In an effort to make PDT a viable treatment in LMICs and LMIC-like settings, here we evaluate a battery-powered LED light source which, in addition to providing reduced costs, could also be independent of plug-in electricity during treatment and be powered using precharged batteries.

The specific goal of this pilot study was to explore the feasibility of a low-cost battery powered broadband LED-based light source for PDT in LMICs by comparing it to a standard monochromatic, relatively costly diode laser as the illumination device. We accomplished this goal by testing the two devices for ALA-PDT *in vivo* in a xenograft murine model of squamous cell carcinoma (SCC). Several frequently occurring cancers in the developing world, such as oral, cervical, and skin, are of SCC origin, and we view this proof-of-principle study as an early step toward implementing PDT in low resource settings to treat these SCCs and related cancers. While typical study endpoints of tumor volume or weight are extremely useful measures of treatment efficacy, they do not provide any insights into the mechanistic aspects and long-term outcomes of a given therapeutic modality. Instead, better quantitative measures and biomarkers are often considered to be better prognostic indicators. Here, we calculated areas of necrosis in PDT-treated tumors and also gauged the extent of PDT-induced hypoxia by immunofluorescence (IFC) staining for the biomarker carbonic anhydrase IX (CAIX) and established alterations in the microvessel density (MVD). These parameters have the potential to predict tumor treatment efficacy[12–15] and provide mechanistic insights into the success or failure of the therapy, enabling early additional or secondary interventions in the future.

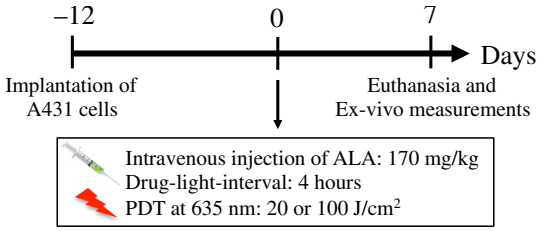

Fig. 1 The timeline for light-emitting diode (LED)-based photodynamic therapy (PDT) study.

2 Materials and Methods

2.1 *Subcutaneous Tumor Implantation*

All animal studies were approved by the Subcommittee on Research Animal Care at the Massachusetts General Hospital and conformed to the guidelines established by the NIH. The protocol for establishing the mouse model was adapted from a previous publication by our group.[16] Briefly, four-to-six-week-old female Swiss nude mice weighing ~20 to 25 g were obtained from Cox Breeding Laboratories, Cambridge, Massachusetts. A431 human epidermoid carcinoma cells of low passage number (<20) in monolayer were collected and resuspended in phosphate buffered saline (PBS), and 50 μl containing 5×10^6 cells were injected subcutaneously into the right scapula region. The tumors were allowed to grow until they reached about 40 to 80 mm^3 in volume (12 days after implantation), at which time point we started the study on tumor response to PDT using the LED light source (LED-PDT) or a laser light source. A schematic timeline of the experimental design and setup is shown in Fig. 1. Tumor response to the treatments was evaluated by daily measuring tumor size in three dimensions with calipers for a total of 7 days. At the end of the experiments, tumors were excised from the sacrificed mice, weighed, measured, and then processed for immunohistochemical analysis. A total of 25 mice were used in the study [five mice in the control (no treatment) group, seven mice in the low-dose (20 J/cm^2) LED-PDT group, five mice in the low-dose laser-PDT group, four mice in the high-dose (100 J/cm^2) LED-PDT group, and four mice in the high-dose laser-PDT group].

2.2 *Photodynamic Therapy*

The tumor-bearing mice were administered ALA intravenously at a dose of 170 mg/kg. After a 4 h interval, transcutaneous irradiation of the tumor through the skin was performed using either the LED or the laser light. For the LED-PDT groups, irradiation was performed using the portable device with a red LED light source (Fig. 2) at a fluence rate of ~60 mW/cm^2 for a designated dose of 20 or 100 J/cm^2. The prototype device used in this study is built in an aluminum box with a

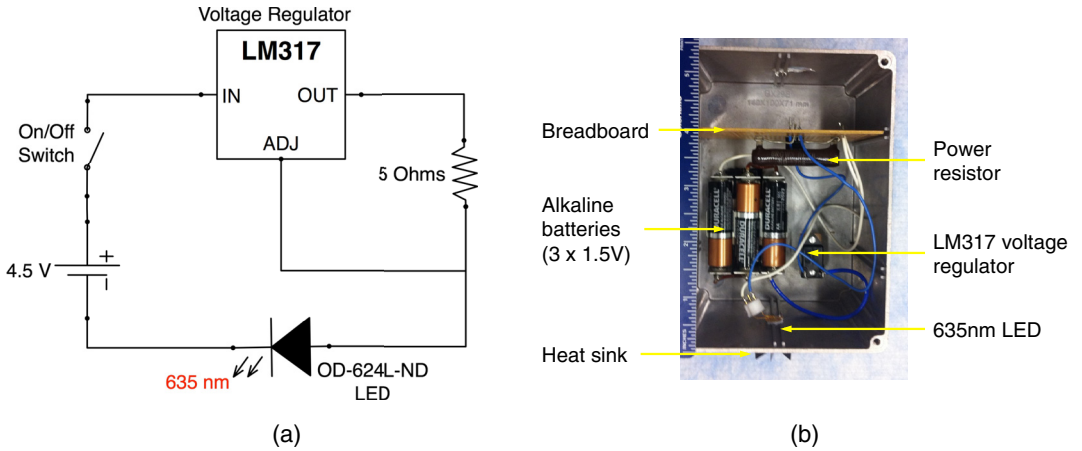

Fig. 2 (a) Electronic circuit and (b) photograph of the battery-powered LED light source.

breadboard slot for electronics and a battery pack for 3 AA batteries (4.5 V). The light source used was a single high-output LED (OptoDiode OD-624L-ND) with peak emission at 635 nm and a full width half maximum of 40 nm built in a TO-39 housing. To manage thermal energy dissipated in the diode, a TO-39 star heat sink was coupled to the LED housing with thermal compound (Wakefield Thermal Solutions, Pelham, New Hampshire). All treatment response data were obtained using three AA alkaline batteries connected in series to power the LED. Internal electronics included a 5Ω power resistor and voltage regulator (LM317, Fairchild Semiconductor) as shown in the Fig. 2(a) circuit diagram. The LM317 is a three-terminal floating regulator and it maintained a nominal 1.25 V reference between its output (OUT) and adjustment (ADJ) terminals. This reference voltage was converted to a constant current by the 5Ω power resistor that flowed through the LED and to the ground.

For the laser-PDT groups, a commercially available laser source (Model 7401; Intense, North Brunswick, New Jersey) operating at 635 nm was used. The output of the laser [measured via a VEGA laser power energy meter (Ophir Laser Measurement Group, LLC)] was adjusted to 60 mW/cm^2 to provide the same fluencerate as the LED light source. The beam diameter for both light sources was ~6 mm in diameter.

2.3 *Hemotoxylin and Eosin Stain and IFC Procedure*

Post-euthanasia, tumors were extracted and embedded in a mold with cryoembedding media (OCT) on dry ice. Sections were cut using a cryostat 250 to 300 μm levels across the entire tumor volume. At each level, two adjacent sections (5 μm each) were stained for standard hemotoxylin and eosin (H&E) stain and IFC stains, respectively. The H&E stain was performed using a Leica ST5010 Autostainer XL to examine tissue morphology (structure). Hematoxylin stained nucleic acids blue and eosin stained the cytoplasm and extracellular matrix pink. IFC staining was performed to obtain information on the microvessel marker (CD31) and CAIX biomarkers. Briefly, after cryostat sectioning, the slides were fixed in a precooled mixture of 1:1 acetone and methanol for 20 min on ice, and then air dried for 30 min at room temperature. The slides were then washed three times (5 min each) in PBS. A protein block (Dako Protein Block Reagent) was applied to the tissue sections for 1 h at room temperature, followed by application of the antibody at 100× dilution overnight at 4°C. Mouse CD31/PECAM-1 Affinity Purified Polyclonal antibody (R&D Systems, Inc.) and human CAIX antibody (Santa Cruz Biotechnology, Inc.) were used for staining the microvasculature and hypoxic areas in the tumor section respectively. The slides were washed in PBS and secondary antibody (Donkey Anti-Goat IgG NL493 Affinity Purified PAb for recognizing CD31 antibody and Donkey Anti-Rabbit NL557 for recognizing CAIX antibody from R&D Systems, Inc.) was applied for 2 h at room temperature. Finally, the slides were washed and sealed with coverslips and nail polish using a SlowFadeGold AntifadeMountant with 4',6-diamidino-2-phenylindole (DAPI) (S36938, Invitrogen).

2.4 *Image Analysis*

A whole slide scanning fluorescence imaging system (Hamamatsu NanoZoomer 2.0-RS) was used to image both H&E and IFC slides. The resolution of the NanoZoomer system is 0.23 μm/pixel. The imaging system has a filter wheel unit that automatically selects and switches filters for excitation and emission wavelengths to allow sequential image acquisition at multiple wavelengths. The NanoZoomer series uses a three-chip time delay integration (TDI) camera to accurately reproduce sample colors. It enables the observation of minute variations in the colors of samples. The three-chip TDI camera has red, green, and blue channels and they are used to produce a single RGB image. The nanozoomer systems stores images in nanozoomer digital pathology image (NDPI) file format, a format developed and used by Hamamatsu, Inc. (for storing image data generated by slide-scanners at different resolutions). In our analysis, we converted the NDPI images to tiffs at 10× magnification using ImageJ NDPI Tools plugin. The tiffs were then analyzed using customized Matlab code and image processing

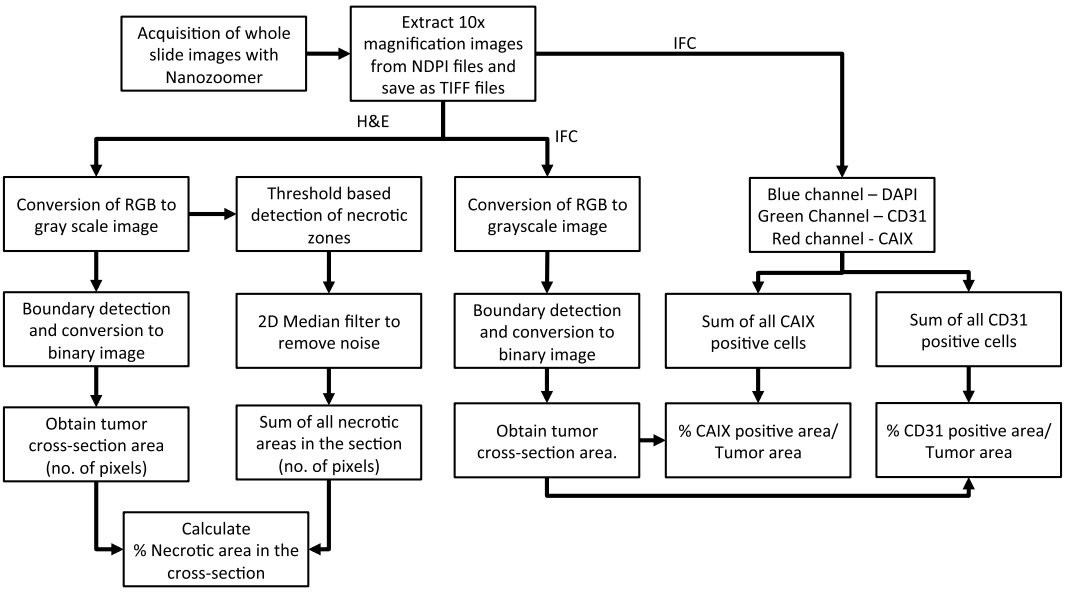

Fig. 3 Flowchart describing the image processing algorithms to obtain percent necrotic volume, percent carbonic anhydrase IX (CAIX)-positive cells, and CD31-positive cells in a tumor cross section.

toolbox functions for the evaluation of necrotic regions, evaluation of MVD (CD31-positive cells per tumor cross-sectional area), and extent of hypoxia (CAIX-positive cells per tumor cross-sectional area). A detailed flowchart of the image analysis is provided in Fig. 3. Specifically for H&E slides, images were converted to a grayscale image such that a value of 0 represents black and a value of 255 represents white. The white, noncellular regions within the tumor cross-sections were identified using threshold equivalent to values greater than a value of 240. A two-dimensional median filter (filter size of 5.0×5.0 pixels) was applied to the image to remove salt-and-pepper noise. All the necrotic region areas were summed using the bwarea function in the MATLAB image processing toolbox. The region props function in the image processing toolbox aided in identifying tumor cross-section areas. The IFC images contained three channels representing the DAPI, CD31, and CAIX stains. To obtain the tumor cross-section area from the IFC images, the RGB fluorescence images were first converted to grayscale using the rgb2gray function in the image processing toolbox of MATLAB. Utilizing "Otsu" threshold algorithm (graythresh function) and the im2bw function, the grayscale images were converted to binary images. The sum of the positive pixels in the binary image yielded the tumor cross-section area. The green and the red channel data were transformed to a binary image to calculate the CD31 and CAIX, respectively, positive regions within the same tumor cross-section. This process was repeated for ~200 tissue cross-sections with H&E stain and ~50 tissue cross-sections for the IFC stain. Statistical analysis was performed using GraphpadPrism (La Jolla, California) and MedCalc (Ostend, Belgium). One-way analysis of variance (ANOVA) Tukey's multiple comparison test (Graphad PRISM) was used to statistically compare the MVD and CAIX expression among different groups and time points. *F*-test (MedCalc) was used to statistically compare the standard deviations of the laser and LED-based PDT groups. A p-value <0.05 was considered to be significant unless specified.

3 Results and Discussion

The tumor volume measurements of mice that underwent laser-PDT or LED-PDT at 20 or 100 J/cm^2 are shown in Fig. 4(a). The tumors in mice that did not receive any treatment [Fig. 4(a), black line] had an exponential growth as expected. On day 2 post-therapy, no significant difference was observed between the tumor volumes in all treatment groups. As a response to PDT, the mice developed some edematic response[17] post-treatment, which resulted in larger tumor volumes 2 days post-PDT. While a significant difference between the tumor volumes of low dose PDT and nontreated groups was observed at 7 days post-therapy, the high-dose PDT group showed a significant difference in tumor volume within 4 days post-therapy. The mice that received higher light doses (100 J/cm^2) had better treatment responses compared to those which received a 20 J/cm^2 light dose, as expected. Indeed, PDT dose and subsequent treatment response are dependent on the light dose utilized in the treatment as has been shown by us and others.[6,18] We also observed no statistical difference (one-way ANOVA) between tumor volumes in mice that underwent Laser or LED-PDT.

Figure 4(b) shows a scatter plot of *ex-vivo* tumor volumes (tumors were extracted 7 days post-therapy) versus post-excision tumor weight for the control mice (black circle), the mice that received 20 J/cm^2 [Fig. 4(b), squares], and mice that received 100 J/cm^2 [Fig. 4(b), triangles]. Tumors that did not receive any treatment [Fig. 4(b), black circle] weighed more than PDT-treated tumors. The tumors treated with 20 J/cm^2 fluence weighed more and had a higher volume than the tumors treated with high light dose (100 J/cm^2). No statistical difference in the weights of the excised tumors between the LED and laser-treated tumors was observed. An *F*-test comparing the standard deviations of the LED and laser-PDT groups yielded a p-value of 0.25 indicating no significant difference between the standard deviations of the two groups.

Higher necrotic volumes are representative of better treatment outcome as has been shown in PDT by our group and others.[17,19–21] To evaluate the efficacy of our LED-based PDT, we compared the necrotic volume in the tumors to those generated by the laser-based PDT. Generally, random representative tissue sections of the tumor are analyzed for calculation of necrotic areas. Here, necrotic areas for ~15 to 25 cross-sections per tumor spaced 250 to 300 μm apart are calculated providing coverage of a large proportion of the tumor. The tumor cross-section area obtained from the H&E images was summed

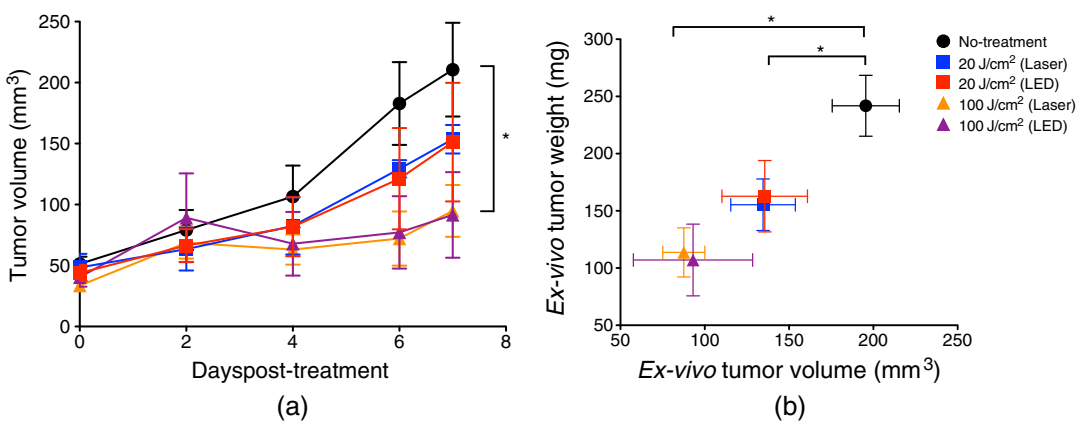

Fig. 4 (a) Longitudinal tumor volume measurements and (b) scatter plot of *ex-vivo* tumor volume (tumors were extracted 7 days post-therapy) versus post-excision tumor weight of mice that underwent no treatment (black circle), low dose (20 J/cm^2) LED-PDT (red square), low dose laser-PDT (blue square), high dose (100 J/cm^2) LED-PDT (purple triangle), and high dose laser-PDT (orange triangle).The error bars represent standard error of the mean (SEM).

to obtain gross tumor volume and was correlated with volume of tumors measured via calipers postexcision [Fig. 5(a)]. A good correlation ($r^2 = 0.81$, p-value <0.001) of tumor volume obtained from H&E images and postexcision tumor volume was observed, indicating that we obtained sufficient sampling of the tumor to draw meaningful conclusions about total necrotic volume in the tumors. Representative H&E images of a tumor treated with LED and laser-PDT at 100 J/cm^2 and control tumor are shown in Figs. 5(c) to 5(e). PDT-treated tumors clearly show enhanced necrotic regions [Fig. 5(c) pointed by a black arrow] while the control (no-treatment) tumor [Fig. 5(e)] had dense viable tissue. Quantification of the necrotic areas within the tumors [Fig. 5(b)] demonstrates that the PDT-treated tumors had significantly higher necrotic areas than the control group (p-value <0.05). Furthermore, we do not observe any significant difference in necrotic volumes between the LED-PDT [Fig. 5(b), purple bar] and laser-PDT [Fig. 5(b), orange bar] groups.

Figure 6 shows representative fluorescence images of tumor sections from mice treated with LED-PDT, laser-PDT, and no-treatment groups. The cell nuclei stained in DAPI are pseudocolored in blue. The blood vessels stained with CD31 biomarker are shown in green and the CAIX biomarker is pseudocolored in red. MVD in various tumors (~15 to 20 cross-sections/group) was quantified via IFC staining of the standard biomarker platelet endothelial cell adhesion molecule (PECAM-1), also known as cluster of differentiation 31 (CD31).[22] No significant differences ($p > 0.05$) between the blood vessel densities of different groups [Fig. 6(d)] were observed. These results are in agreement with several studies that indicate no change in MVD post ALA-based PDT and support a general belief that ALA-PDT destruction mechanisms may be dominated by cellular rather than vascular damage.[23,24] However, this may not be the entire explanation for the observation. The MVDs were determined at 7 days post-treatment, and it is conceivable that there was enough time for vessel regrowth in which there should have been a vascular component to the PDT-induced damage, as has been suggested by others.[25–27]

Figures 6(a) and 6(b) show enhanced CAIX expression in tumors treated with PDT. Quantitative analysis of the number of CAIX-positive cells in various tumor cross-sections indicated CAIX expression is significantly higher in the PDT-treated tumors than in tumors of the no-treatment group ($p < 0.05$). The LED-PDT [Fig. 6(e), purple bar] or the laser-PDT [Fig. 6(e), orange bar] groups did not have significant difference in CAIX-positive cells per tumor cross-section. Several studies have shown that tumors experience hypoxic conditions within a few minutes to several hours post-PDT.[28,29] PpIX is primarily a type II photosensitizer that generates cytotoxic species via consumption of oxygen in the surrounding environment leading to hypoxic conditions.[30] CAIX is a downstream biomarker of hypoxia inducible factor (HIF-1α), upregulated under hypoxic conditions, making CAIX closely associated with hypoxia.[31–33] Our observation of high CAIX expression in PDT-treated tumors is consistent with the expectation that photodynamic action would create a hypoxic environment.

PDT dosimetry can be complex and several groups have pointed to a strong dependence on light delivery parameters.[18,34–36] Therefore, there was no *a priori* assumption that

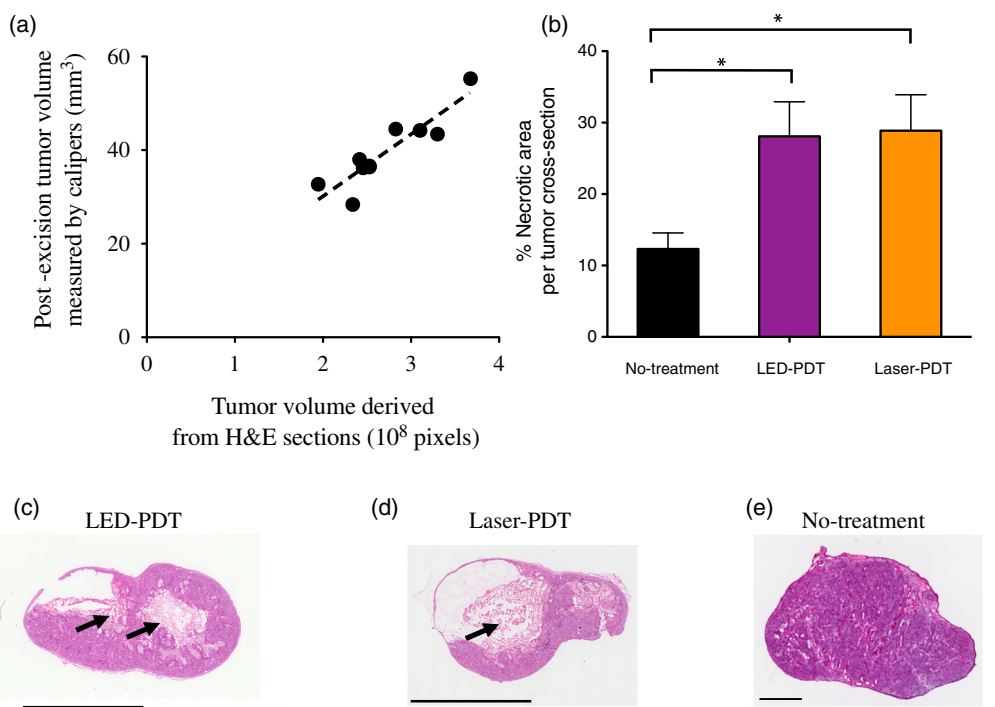

Fig. 5 (a) Scatter plot showing correlation between tumor volume deduced from the hemotoxylin and eosin (H&E) tissue sections and postexcision tumor volume measured with calipers. The solid black line represents a linear correlation with $r^2 = 0.81$. (b) Mean necrotic area per tumor cross-section area in various mice in the no-treatment ($n = 74$ sections), LED-PDT ($n = 48$ sections), and laser-PDT ($n = 40$ sections) groups. The error bars represent SEM. The PDT-treated group had higher necrotic area than the control groups. There was no statistical difference (one-way analysis of variance test) between the LED-PDT and laser-PDT groups. (c–e) Representative H&E images from mice in the LED-PDT, laser-PDT, and no-treatment groups. The scale bar represents length of 5 mm.

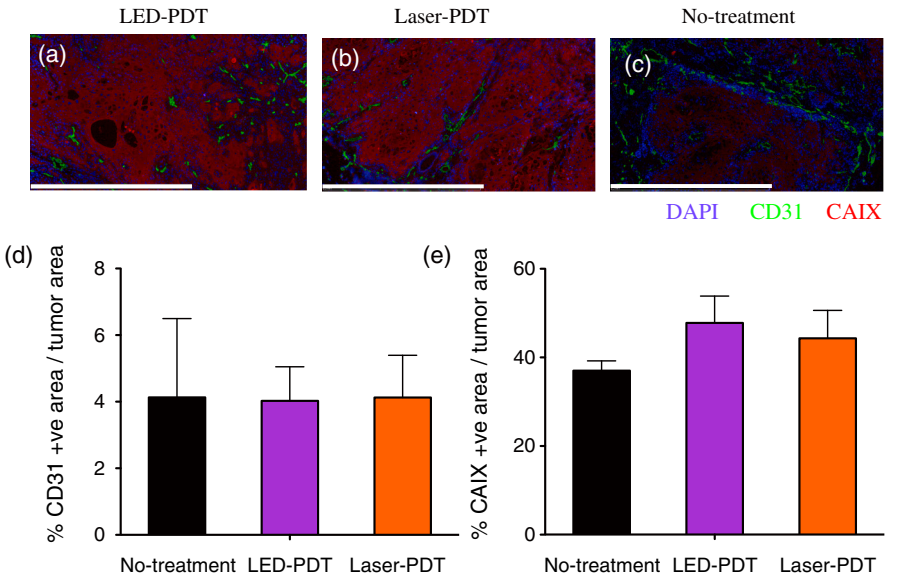

Fig. 6 (a–c) Representative immunofluorescence images of the tumors in the LED-PDT, laser-PDT and no-treatment. The scale bar represents length of 1 mm. The cell nuclei stained in DAPI are pseudo-colored in blue. The blood vessels stained with CD31 biomarker are shown in green and the CAIX biomarker is pseudo-colored in red. We notice an enhancement in CAIX fluorescence signal (red) in PDT treated tumors. (d and e) Graphs showing microvessel density and percent CAIX-positive area per tumor cross-section across different cross-sections in the tumors from various groups. There was no statistically significant difference in MVD between the groups. The PDT-treated tumors had higher CAIX-positive area than the control tumors. There was no statistically significant difference in percent CAIX-positive area per tumor cross-section between the LED-PDT and laser-PDT group.

using the broadband LED-based source would quantitatively yield the same results as the monochromatic laser light source. It is encouraging and a bit surprising to us that in this comparative *in vivo* study on the biological outcomes of PDT, using a low-cost LED-based battery powered source and a traditional 635-nm laser source gave identical results in all the parameters evaluated despite these sources having contrasting spectral, coherence, and power stability properties that may well have affected the treatment outcomes. This initial study with a mobile, low-cost, battery-powered broadband light source points to the feasibility of PDT in low resource settings. Here, we measured the LED power before treating every mouse and replaced the batteries of the light source before treatment of the mice if the degradation of power was >10%. It is clear that studies aimed at improving the illumination device along with ALA dose and routes of administration are needed to define a reliable set of treatment conditions in a low-resource setting. In addition to the standard method of continuous illumination during PDT, the battery-powered light source could also be adapted with an "on-off" switch to perform fractionated PDT, a methodology that has shown potential for various tumors.[37–39] Studies regarding the stability of the device for longer illumination times or fractionated PDT are currently being investigated.

The study was designed to qualitatively and quantitatively compare the two light sources—battery powered LED and traditional commercially available laser—for therapeutic efficacy in an *in vivo* model and was not designed to achieve complete eradication of tumors. As it turned out, there was no difference between any of the parameters evaluated for treatment response between the two sources. Consistent with previous reports pointing to the importance of PDT dose in modulating the treatment outcome,[6,36,40–42] we observed regions of viable tumor [Fig. 4(a)] even at a high incident dose of 100 J/cm^2 possibly due to heterogeneous PpIX accumulation or light distribution. This effect of tumor heterogeneity is a barrier to almost all cancer therapeutics. In the context of ALA-PDT, we have several ongoing strategies that may overcome the heterogeneous PpIX distribution.[43] Often, fluorescence imaging of PpIX is used as a dosimetric parameter and the change in PpIX fluorescence post-therapy, i.e., the photobleaching of PpIX, has been useful in personalizing therapeutic dose and providing better insights into treatment efficacy. Along with low-cost light sources similar to the one described here, portable imaging systems, including potential smart phone based devices for fluorescence imaging techniques,[44–48] combined with strategies for more homogeneous PpIX synthesis might provide rapid and inexpensive options for therapy and monitoring design in LMICs.

4 Conclusions

This study demonstrates identical results not only in tumor volumes but also in the biomarker metrics such as necrotic volume, microvascular density, and CAIX expression (measure of hypoxia) with both the portable, battery-powered LED light source and the traditional laser light source post ALA-based PDT in SCC tumors. These results are promising and merit comprehensive studies to (1) investigate appropriate light delivery parameters (e.g., time and irradiance), (2) evaluate the LED light source in other models of cancer relevant to LMICs, and (3) develop strategies to overcome heterogeneity of PpIX distribution within tumors. With the aid of battery-powered light sources and photosensitizer prodrugs, such as ALA, which can be stored at room temperature and administered via oral beverages, PDT could be an important treatment option in the treatment of oral, cervical, skin, and other cancers that are prevalent in LMICs.

The current mainstays of cancer treatments, including surgery, radiation, and chemotherapy, are either not accessible to a majority of patients or not affordable. These traditional approaches require hospitalization or monitoring at medical centers with infrastructure. Therefore, innovative, low-cost approaches with potential for use in low resource settings that are universal and not only confined to LMICs are critical to meet the impending challenge. With low-cost light sources, PDT offers one such alternative. Although several issues remain before the technology that can be made reliable and portable for use in low resource settings, the present study is a first step toward this translation.

Acknowledgments

This work was supported by NIH grants F32CA165881 (Mallidi), 1K99CA175292 (Rizvi), R00CA155045 (Celli), UH2CA189901 (Hasan and Celli) and 5P01CA084203 (Hasan). The authors thank Dr. Jie Zhao and Mrs. Winxing Lin at the Wellman Center Photopathology core for cryo-cutting the samples. We also thank Dr. Rehab Amin for assisting the authors with immunofluorescence stains, Dustin P. Jones, Abdelali Ziouche and Gwendolyn Cramer at University of Massachusetts Boston for fabrication and characterization of the LED light source and Zachary Simpson at Wellman Center for assistance with editing.

References

1. E. Bender, "Developing world: global warning," *Nature* **509**(7502), S64–S65 (2014).
2. F. Bray et al., "Global cancer transitions according to the Human Development Index (2008–2030): a population-based study," *Lancet Oncol.* **13**(8), 790–801 (2012).
3. P. Farmer et al., "Expansion of cancer care and control in countries of low and middle income: a call to action," *Lancet* **376**(9747), 1186–1193 (2010).
4. J. Ferlay et al., "Estimates of worldwide burden of cancer in 2008: GLOBOCAN 2008," *Int. J. Cancer* **127**(12), 2893–2917 (2010).
5. C. Are et al., "A review of global cancer burden: trends, challenges, strategies, and a role for surgeons," *J. Surg. Oncol.* **107**(2), 221–226 (2013).
6. J. P. Celli et al., "Imaging and photodynamic therapy: mechanisms, monitoring, and optimization," *Chem. Rev.* **110**(5), 2795–2838 (2010).
7. Z. Huang et al., "Photodynamic therapy: an update on clinical applications," *J. Innov. Opt. Health Sci.* **02**(01), 73–92 (2009).
8. B. C. Wilson, M. S. Patterson, and L. Lilge, "Implicit and explicit dosimetry in photodynamic therapy: a new paradigm," *Lasers Med. Sci.* **12**(3), 182–199 (1997).
9. T. J. Dougherty et al., "Photodynamic therapy," *J. Natl Cancer Inst.* **90**(12), 889–905 (1998).
10. T. S. Mang, "Lasers and light sources for PDT: past, present and future," *Photodiagn. Photodyn. Ther.* **1**(1), 43–48 (2004).
11. J.-C. Tsai et al., "Photodynamic therapy of oral dysplasia with topical 5-aminolevulinic acid and light-emitting diode array," *Lasers Surg. Med.* **34**(1), 18–24 (2004).
12. J. Garcia-Donas et al., "Prospective study assessing hypoxia-related proteins as markers for the outcome of treatment with sunitinib in advanced clear-cell renal cell carcinoma," *Ann. Oncol.* **24**(9), 2409–2414 (2013).
13. P. C. McDonald and S. Dedhar, "Carbonic anhydrase IX (CAIX) as a mediator of hypoxia-induced stress response in cancer cells," *Subcell. Biochem.* **75**, 255–269 (2014).
14. M. Kappler et al., "Immunohistochemical detection of HIF-1alpha and CAIX in advanced head-and-neck cancer. Prognostic role and correlation with tumor markers and tumor oxygenation parameters," *Strahlenther Onkol* **184**(8), 393–399 (2008).
15. P. J. Hoskin et al., "GLUT1 and CAIX as intrinsic markers of hypoxia in bladder cancer: relationship with vascularity and proliferation as predictors of outcome of ARCON," *Br. J. Cancer* **89**(7), 1290–1297 (2003).
16. S. Anand, T. Hasan, and E. V. Maytin, "Mechanism of differentiation-enhanced photodynamic therapy for cancer: upregulation of coproporphyrinogen oxidase by C/EBP transcription factors," *Mol. Cancer Ther.* **12**(8), 1638–1650 (2013).
17. B. Chen et al., "Combining vascular and cellular targeting regimens enhances the efficacy of photodynamic therapy," *Radiat. Oncol. Biol.* **61**(4), 1216–1226 (2005).
18. B. W. Henderson, T. M. Busch, and J. W. Snyder, "Fluence rate as a modulator of PDT mechanisms," *Lasers Surg. Med.* **38**(5), 489–493 (2006).
19. C. Sheng et al., "Assessment of photosensitizer dosimetry and tissue damage assay for photodynamic therapy in advanced-stage tumors," *Photochem. Photobiol.* **79**(6), 520–525 (2004).
20. M. T. Huggett et al., "Phase I/II study of verteporfin photodynamic therapy in locally advanced pancreatic cancer," *Br. J. Cancer* **110**(7), 1698–1704 (2014).
21. F. F. Jiang et al., "Photodynamic therapy of U87 human glioma in nude rat using liposome-delivered photofrin," *Lasers Surg. Med.* **22**(2), 74–80 (1998).
22. B. Q. Spring et al., "Efficient measurement of total tumor microvascularity ex vivo using a mathematical model to optimize volume subsampling," *J. Biomed. Opt.* **18**(9), 096015 (2013).
23. M. A. Herman, D. Fromm, and D. Kessel, "Tumor blood-flow changes following protoporphyrin IX-based photodynamic therapy in mice and humans," *J. Photochem. Photobiol. B* **52**(1–3), 99–104 (1999).
24. B. W. Pogue et al., "Tumor PO(2) changes during photodynamic therapy depend upon photosensitizer type and time after injection," *Comp. Biochem. Physiol. A Mol. Integr. Physiol.* **132**(1), 177–184 (2002).
25. D. Roberts et al., "Tumor vascular shutdown following photodynamic therapy based on polyhematoporphyrin or 5-aminolevulinic acid," *Int. J. Oncol.* **5**(4), 763–768 (1994).
26. T. L. Becker et al., "Monitoring blood flow responses during topical ALA-PDT," *Biomed. Opt. Express* **2**(1), 123–130 (2011).
27. T. A. Middelburg et al., "Topical photodynamic therapy using different porphyrin precursors leads to differences in vascular photosensitization and vascular damage in normal mouse skin," *Photochem. Photobiol.* **90**(4), 896–902 (2014).
28. B. W. Henderson and V. H. Fingar, "Relationship of tumor hypoxia and response to photodynamic treatment in an experimental mouse tumor," *Cancer Res.* **47**(12), 3110–3114 (1987).
29. S. Iinuma et al.," *In vivo* fluence rate and fractionation effects on tumor response and photobleaching: photodynamic therapy with two photosensitizers in an orthotopic rat tumor model," *Cancer Res.* **59**(24), 6164–6170 (1999).
30. B. W. McIlroy et al., "Spatial measurement of oxygen levels during photodynamic therapy using time-resolved optical spectroscopy," *J. Photochem. Photobiol. B* **43**(1), 47–55 (1998).
31. S. Yanase et al., "Synergistic interaction of 5-aminolevulinic acid-based photodynamic therapy with simultaneous hyperthermia in an osteosarcoma tumor model," *Int. J. Oncol.* **29**(2), 365–373 (2006).
32. S. E. Rademakers et al., "Metabolic markers in relation to hypoxia; staining patterns and colocalization of pimonidazole, HIF-1α, CAIX, LDH-5, GLUT-1, MCT1 and MCT4," *BMC Cancer* **11**(1), 167 (2011).
33. S. Teppo et al., "The hypoxic tumor microenvironment regulates invasion of aggressive oral carcinoma cells," *Exp. Cell Res.* **319**(4), 376–389 (2013).
34. I. Rizvi et al., "PDT dose parameters impact tumoricidal durability and cell death pathways in a 3D ovarian cancer model," *Photochem. Photobiol.* **89**(4), 942–952 (2013).
35. T. H. Foster et al., "Fluence rate effects in photodynamic therapy of multicell tumor spheroids," *Cancer Res.* **53**(6), 1249–1254 (1993).
36. B. C. Wilson and M. S. Patterson, "The physics, biophysics and technology of photodynamic therapy," *Phys. Med. Biol.* **53**(9), R61–R109 (2008).
37. H. S. de Bruijn et al., "Improvement of systemic 5-aminolevulinic acid-based photodynamic therapy *in vivo* using light fractionation with a 75-minute interval," *Cancer Res.* **59**(4), 901–904 (1999).
38. A. Curnow et al., "Light dose fractionation to enhance photodynamic therapy using 5-aminolevulinic acid in the normal rat colon," *Photochem. Photobiol.* **69**(1), 71–76 (1999).

39. M. D. Glidden, "Image-based quantification of benzoporphyrin derivative uptake, localization, and photobleaching in 3D tumor models, for optimization of PDT parameters," *Theranostics* **2**(9), 827–839 (2012).
40. K. K.-H. K. Wang, S. S. Mitra, and T. H. T. Foster, "A comprehensive mathematical model of microscopic dose deposition in photodynamic therapy," *Med. Phys.* **34**(1), 282–293 (2007).
41. A. R. Oseroff et al., "Treatment of diffuse basal cell carcinomas and basaloid follicular hamartomas in nevoid basal cell carcinoma syndrome by wide-area 5-aminolevulinic acid photodynamic therapy," *Arch. Dermatol.* **141**(1), 60–67 (2005).
42. E. W. Jeffes et al., "Photodynamic therapy of actinic keratosis with topical 5-aminolevulinic acid. A pilot dose-ranging study," *Arch. Dermatol.* **133**(6), 727–732 (1997).
43. S. Anand et al., "Vitamin D3 enhances the apoptotic response of epithelial tumors to aminolevulinate-based photodynamic therapy," *Cancer Res.* **71**(18), 6040–6050 (2011).
44. Q. Wei et al., "Fluorescent imaging of single nanoparticles and viruses on a smart phone," *ACS Nano* **7**(10), 9147–9155 (2013).
45. L. Shen, J. A. Hagen, and I. Papautsky, "Point-of-care colorimetric detection with a smartphone," *Lab Chip* **12**(21), 4240–4243 (2012).
46. E. Jonathan and M. Leahy, "Investigating a smartphone imaging unit for photoplethysmography," *Physiol. Meas.* **31**(11), N79–N83 (2010).
47. J. Canning et al., "Measurement of fluorescence in a rhodamine-123 doped self-assembled 'giant' mesostructured silica sphere using a smartphone as optical hardware," *Sensors* **11**(7), 7055–7062 (2011).
48. H. Zhu et al., "Cost-effective and compact wide-field fluorescent imaging on a cell-phone," *Lab Chip* **11**(2), 315–322 (2011).

Srivalleesha Mallidi is a biomedical engineer trained in custom building multi-modality ultrasound and optical imaging systems. After graduation, she joined Wellman Center for Photomedicine with a goal to translate the imaging techniques to clinic, and is currently a NIH Ruth L. Kirschstein postdoctoral fellow. Her research interests are in the fields of ultrasound imaging, photoacoustic imaging, nano-molecular imaging, image-guided therapeutics, photodynamic therapy, and combination treatments.

Zhiming Mai received his PhD degree in molecular biology and immunology, and since then he has been trained in cancer biology in Harvard-affiliated Hospitals. His research interest is to evaluate photodynamic therapy-based combinations in animal models for tumors, and to seek optimal approaches to manage those diseases.

Imran Rizvi is trained in tumor biology and engineering sciences. His research focuses on developing bioengineered tumor models to evaluate photodynamic therapy-based combinations in 3D systems and in animal models for cancer.

Joshua Hempstead is a research assistant in the laboratory of Dr. Jonathan Celli at the University of Massachusetts at Boston, where he expects to receive his BS degree in physics in 2015. His current research is centered on development and evaluation of low-cost LED sources for photodynamic therapy and smartphone-based photosensitizer imaging in epidermoid carcinoma tumor models.

Stephen Arnason is an associate professor of physics at the University of Massachusetts Boston. His research focuses on the interplay of microstructure with quantum interactions in thin film material systems. His present research concerns fluctuation spectroscopy in electron glass materials that have been pushed out of equilibrium. He received his PhD degree from Stanford University and completed postdoctoral training at the University of Florida.

Jonathan Celli is currently an assistant professor in the Department of Physics at the University of Massachusetts Boston. His research group draws on physics-based techniques and analysis in cancer research, with an emphasis on photodynamic therapy (PDT). He received his PhD degree in physics from Boston University in 2007 and postdoctoral training in photomedicine and translational cancer research at the Massachusetts General Hospital and Harvard Medical School.

Tayyaba Hasan is a professor of dermatology at Harvard Medical School and a professor of health sciences and technology (Harvard-MIT). The focus of her research is in photochemistry and photodynamic therapy of cancer and infections with over 200 publications in this field. She is inventor of the FDA approved photodynamic treatment of age-related macular degeneration. She leads an NCI-funded international consortium (UH2/UH3 award) on developing low cost enabling technologies for image guided photodynamic therapy of oral cancer.